Advances in Science and Technology Research Journal

Advances in Science and Technology Research Journal, 2026, 20(7), 470–493
https://doi.org/10.12913/22998624/219825
ISSN 2299-8624, License CC-BY 4.0

Received: 2026.01.19
Accepted: 2026.05.15
Published: 2026.06.01

Stability and strength of cold-formed C-shaped and Z-shaped profiles: Analytical studies

Mikołaj Jan Smyczynski[1*], Marcin Rodak[1], Piotr Paczos[1], Jarosław Pruszyński[2], Robert Cep[3]

[1] Institute of Applied Mechanics, Poznan University of Technology, Jana Pawla II 24 Street, 60-965 Poznan, Poland
[2] Zaprom Ltd, Tołcze 3D, 18-106 Tołcze, Poland
[3] Faculty of Mechanial Engineering, VSB- Technical University of Ostrava, 17. Listopadu 2172/15, 708 00 Ostrava 8, Czech Republic
* Corresponding author's e-mail: mikolaj.smyczynski@put.poznan.pl

ABSTRACT

This article presents analytical studies of the stability and strength of thin-walled beams with non-standard cross-sectional geometry, manufactured by Zaprom Ltd. The analyses cover four load conditions, for which critical buckling load values were determined. The studies were conducted for three example beams made of innovative profiles designed to improve structural performance. The paper utilizes an approach combining theory based on the principle of conservation of potential energy with numerical analysis using the finite-stripe method (FSM). The results allow for an assessment of the influence of loading conditions and geometric parameters on the forms of instability and critical load values. The analyses provide a basis for further optimization of the thin-walled profile shapes, taking into account both load-bearing efficiency and structural safety.

Keywords: thin-walled beam, stability, analytical studies, buckling.

INTRODUCTION

Thin-walled beams are an essential component of many modern engineering structures due to their favorable strength-to-weight ratio. However, their slender geometry makes them particularly susceptible to buckling, which can lead to a sudden loss of structural stability. Accurately predicting the buckling capacity of thin-walled beams requires advanced analytical methods that consider both the geometric nature of the cross-section and the influence of boundary conditions and loads. Analytical studies in this field have explored different aspects of stability, including elastic, dynamic, and thermal buckling, using various theoretical and numerical methods.

Hancock (1) conducted a comprehensive review and provided a synthesis of the principal research advancements in cold-formed steel structures published between 1999 and 2001. Pawlak et al. (2) presented the existing body of knowledge concerning geometric imperfections in thin-walled steel members with altered cross-sectional configurations. Magnucka-Blandzi (3) described the effective shaping of cold-formed thin-walled channel beams with double-box flanges subjected to pure bending. Magnucka-Blandzi et al. (4) provided a detailed description of the optimal geometric configuration of cold-formed thin-walled channel beams with double-box flanges under pure bending conditions. Jasion et al. (5) performed both numerical simulations and experimental investigations to evaluate the buckling and post-buckling response of selected cold-formed C-sections with modified geometries, and subsequently compared the results with those obtained for a conventional profile. Rhodes and Seah (6) examined the buckling response of cold-formed thin-walled steel beams with edge stiffeners under pure bending moment loading.

Laudiero and Zaccaria (7) reported numerical determinations of the critical buckling loads for elastic, prismatic thin-walled open-section beams subjected to arbitrary distributions of conservative static loading. Adany and Schafer (8) outlined the formulation of a proposed approach enabling the decomposition of stability buckling modes in single-branched, open-section thin-walled members into pure bending components using the finite strip method. Pawlak et al. (9) investigated both experimentally and numerically the load-bearing capacity and stability resistance of thin-walled channel columns. SudhirSastry et al. (10) conducted a lateral buckling assessment of cold-formed thin-walled channel beams for various configurations of geometric parameters. Grenda and Paczos (11) examined the local elastic buckling response and ultimate load capacity of non-standard thin-walled channel beams under pure bending conditions. Bourihane et al. (12) provided an assessment of the stability behaviour of thin-walled open-section beams subjected to arbitrary loading conditions. Chu et al. (13) carried out a numerical investigation into the local and distortional buckling response of cold-formed steel Z-section beams subjected to uniformly distributed transverse loading. Kim et al. (14) analysed the coupled stability behaviour of thin-walled composite beams with closed cross-sections under various loading conditions using a numerical approach. Hancock and Pham (15) developed the Semi-Analytical Finite Strip Method (SAFSM) for thin-walled sections subjected to localized loading in order to examine web crippling effects. The underlying SAFSM formulation was first outlined, after which the method was applied to the buckling analysis of plates and channel sections under localized load conditions. Pham et al. (16) presented an extensive analytical and numerical investigation into the elastic buckling behaviour of thin-walled channel sections subjected to various combinations of bending and shear stresses. Magnucki et al. (17) conducted analytical, numerical, and experimental investigations into the global and local stability behaviour of thin-walled channel beams with drop flanges. Penava et al. (18) examined the elastic stability behaviour of steel thin-walled C- and Z-section beams in the absence of lateral bracing. Samanta and Kumar (19) investigated the distortional buckling behaviour of simply supported monosymmetric I-beams subjected to three loading scenarios: a mid-span concentrated load, a uniformly distributed load, and a constant sagging bending moment. Silvestre and Camotim (20) outlined the derivation of fully analytical expressions grounded in Generalised Beam Theory (GBT) to determine distortional critical lengths and bifurcation stress resultants for cold-formed steel C- and Z-section members subjected to uniform compression, pure bending, and their combined action. Silva et al. (21) analyzed the web-crippling capacity of cold-formed SFHZ beams under ETF and ITF loading conditions using experimental tests and finite element models. Hulka et al. (22) investigated resistance spot welding (RSW) as a method for connecting thin-walled cold-formed steel elements in lightweight beams made of corrugated galvanized sheets and channel sections. It analyzes how welding parameters affect the microstructure and mechanical properties of low-carbon galvanized steel joints. Pavlovic et al. (23) investigated the stochastic vibration response of a viscoelastic nanobeam subjected to axial loading within the framework of the higher-order nonlocal strain gradient theory, employing the Lyapunov functional method for the analysis. Yu et al. (24) conducted an analytical investigation of the distortional buckling behaviour of cold-formed steel channel-section beams containing circular web openings, based on a modified version of Hancock's solution. Magnucka-Blandzi (25) provided an analytical description of the lateral buckling behaviour of thin-walled beams subjected to combined loading conditions. Korobeynikov et al. (26) investigated the buckling behaviour of nanostructures by applying stability criteria formulated for discrete elastic systems. Binh et al. (27) proposed an enhanced generalized framework, grounded in the energy method, for the stability analysis of thin-walled beams subjected to combined symmetric loading.

In this paper analytical studies on the stability of thin-walled beams cover various aspects, including buckling behavior and effects of different loading conditions. The purpose of this article is to present the results of analytical buckling studies of thin-walled beams, with particular emphasis on various forms of instability and their dependence on structural parameters.

The study addresses thin-walled steel beams with non-conventional cross-sectional configurations, proposing novel profile geometries aimed at enhancing structural performance. These sections are manufactured by Zaprom Ltd. The tests

are aimed at checking the strength of the proposed profiles under specific load conditions. The research combines theoretical formulations derived from the principle of potential energy conservation with numerical simulations conducted using the finite strip method (FSM).

ANALYTICAL STUDIES

The factor influencing the load-bearing capacity of thin-walled bars and beams is the phenomenon of loss of stability. In the case of thin-walled bars/beams, we can distinguish three forms of buckling:

- General or global, which characterizes in the case of a rod its flexural, torsional or flexural-torsional buckling, while in the case of bent beams its lateral-torsional buckling. The shape of the cross-section does not change after buckling,
- Local, characterised by deformation of the beam cross-section, while in members with flat plates the junction lines between the walls remain stationary,
- Distortional, which, similarly to the local form of buckling, is characterized by cross-section deformation, but the edges connecting two flat walls can move.

The study considers beams of length L, pinned at both ends and loaded with:

a) Two moments of value M applied to both ends of the beam (pure bending) – load case I (Figure 1). The values of external forces distributed along the length of the beam are:

$$q_x = 0,\ q_y = 0,\ q_z = 0. \tag{1}$$

Internal forces are equal to:

$$N(x)=0,\ M_y(x)=M=M_{max},\ M_z(x)=0,\ B=0. \tag{2}$$

b) Uniformly distributed transverse load of intensity q in the plane passing through the shear center – load case II (Figure 2). The values of external forces distributed along the length of the beam are:

$$q_x = 0,\ q_y = 0,\ q_z = q. \tag{3}$$

while internal forces:

$$N(x) = 0,\ M_y(x) = 4M_{max}x/L(1–x/L),\quad M_z(x) = 0,\ B = 0, \tag{4}$$

where:

$$M_{max} = 1/8\ qL^2. \tag{5}$$

c) Concentrated force F applied halfway along the beam at the shear center – load case III (Figure 3). The values of external forces distributed along the length of the beam are:

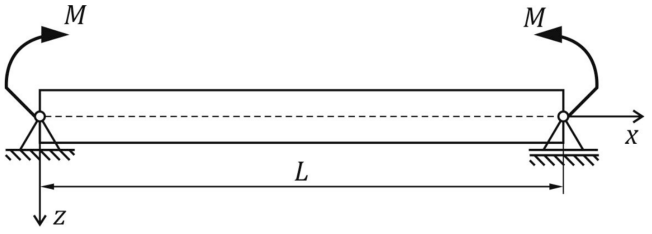

Figure 1. Loading diagram – pure bending

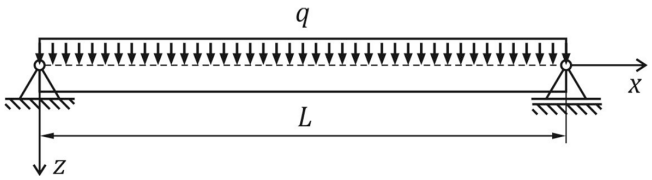

Figure 2. Load diagram – load with uniformly distributed force q

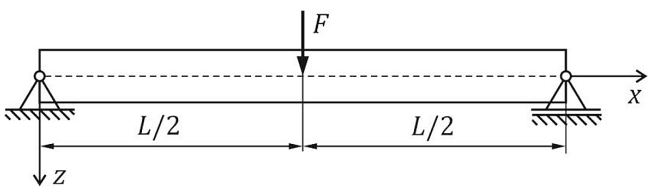

Figure 3. Load diagram – load with concentrated force F

$$q_x = 0, \quad q_y = 0, \quad q_z = F\delta\left(x - \frac{L}{2}\right), \tag{6}$$

The internal forces are equal to:

$$N(x) = 0, \quad M_y(x) = 2M_{max} \times \begin{cases} \frac{x}{L} & \text{for} \quad x \in \langle 0, \frac{L}{2} \rangle \\ 1 - \frac{x}{L} & \text{for} \quad x \in \langle \frac{L}{2}, L \rangle \end{cases}, \quad M_z(x) = 0, \quad B = 0, \tag{7}$$

where:

$$M_{max} = \frac{1}{4}FL. \tag{8}$$

d) longitudinal force P applied in the middle of the cross-section – load case IV (Figure 4).

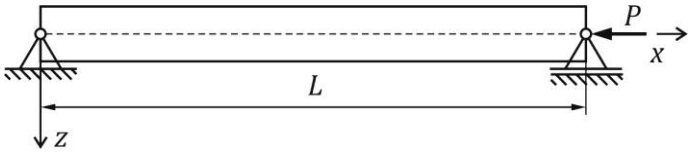

Figure 4. Load diagram – load with longitudinal force P

The values of external forces distributed along the length of the beam are:

$$q_x = 0, \quad q_y = 0, \quad q_z = 0. \tag{9}$$

The internal forces are equal to:

$$N(x) = -P, \quad M_y(x) = 0, \quad M_z(x) = 0, \quad B = 0. \tag{10}$$

Second-order equilibrium equations

A Cartesian coordinate system (x,y,z) was adopted to characterise the displacement field of the analysed thin-walled beams, with the x-axis aligned along the beam longitudinal axis, and the y and z axes defining the centroidal coordinate system of each cross-section (Figure). The displacements of any point P in the x, y and z axes directions were designated u_P, v_P, w_P. The displacement of the centre of cross-section C in the x-axis direction was designated $u_C = u$, while the displacement of the shear centre S in the y and z axes directions was designated $v_S = v$ and $w_S = w$, respectively. Furthermore, it was assumed that the points lying on the line with coordinates (x, y_R, z_R) are elastically supported and the rotation in the direction parallel to the x-axis is limited. The following geometric properties of cross-sections are defined:

- A – surface area,
- J_s – geometric characteristic for free torsion,
- J_y, J_z, J_{yz} – axial moments of inertia,
- J_ω – segmental moment of inertia,
- r_S^2 – polar radius of gyration relative to the shear center,
- $\beta_{Sy}, \beta_{Sz}, \beta_\omega$ – cross-section asymmetry arms.

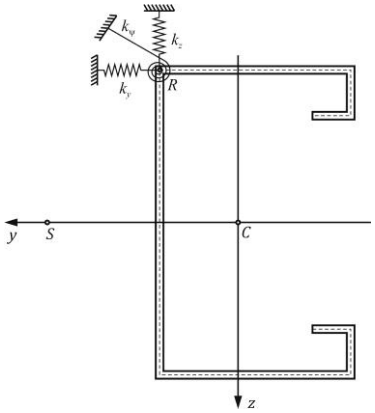

Figure 5. Beam cross-section (28)

The equilibrium equations for a thin-walled beam were determined from the principle of minimum total potential energy

$$\delta(U_\varepsilon - W) = 0, \tag{11}$$

where: U_ε is the elastic deformation energy, while W is the work of the load.

Potential energy of elastic deformation (Mohri et al. (29), Li (30)) is written in the form:

$$U_\varepsilon = U_{\varepsilon l} + U_{\varepsilon n}, \tag{12}$$

where:

$$\begin{aligned} U_{\varepsilon l} = {} & \frac{1}{2}E\int_0^L \left[A\left(\frac{\mathrm{d}u}{\mathrm{d}x}\right)^2 + J_z\left(\frac{\mathrm{d}^2v}{\mathrm{d}x^2}\right)^2 + 2J_{yz}\frac{\mathrm{d}^2v}{\mathrm{d}x^2}\frac{\mathrm{d}^2w}{\mathrm{d}x^2} + J_y\left(\frac{\mathrm{d}^2w}{\mathrm{d}x^2}\right)^2 + J_\omega\left(\frac{\mathrm{d}^2\psi}{\mathrm{d}x^2}\right)^2\right]\mathrm{d}x \\ & + \frac{1}{2}G\int_0^L J_s\left(\frac{\mathrm{d}\psi}{\mathrm{d}x}\right)^2\mathrm{d}x + \frac{1}{2}\int_0^L \left[k_y v_R^2 + k_z w_R^2 + k_\psi \psi^2\right]\mathrm{d}x \end{aligned} \tag{13}$$

$$\begin{aligned} U_{\varepsilon n} = {} & \frac{1}{2}\int_0^L N\left[\left(\frac{\mathrm{d}v}{\mathrm{d}x}\right)^2 + \left(\frac{\mathrm{d}w}{\mathrm{d}x}\right)^2\right]\mathrm{d}x + \frac{1}{2}\int_0^L \left[r_S^2 N + 2\beta_{Sz}M_y - 2\beta_{Sy}M_z + 2\beta_\omega B\right]\left(\frac{\mathrm{d}\psi}{\mathrm{d}x}\right)^2\mathrm{d}x \\ & + \int_0^L \left[M_y\frac{\mathrm{d}^2v}{\mathrm{d}x^2} + M_z\frac{\mathrm{d}^2w}{\mathrm{d}x^2}\right]\psi\mathrm{d}x + \int_0^L N\left[z_S\frac{\mathrm{d}v}{\mathrm{d}x} - y_S\frac{\mathrm{d}w}{\mathrm{d}x}\right]\frac{\mathrm{d}\psi}{\mathrm{d}x}\mathrm{d}x, \end{aligned} \tag{14}$$

The work of external forces is:

$$W = \int_0^L \left(-q_x u + q_y v_Q + q_z v_Q\right)dx - M_y\frac{\mathrm{d}w}{\mathrm{d}x}\Big|_0^L + M_z\frac{\mathrm{d}v}{\mathrm{d}x}\Big|_0^L + Nu|_0^L, \tag{15}$$

where v_Q and w_Q is the displacement of points lying on the axis $Q(x, y_Q, z_Q)$ to which forces of intensity q_y, q_z are applied. From the principle of minimum total potential energy, a system of second-order differential equations was obtained:

$$\begin{aligned} & EA\frac{\mathrm{d}^2u}{\mathrm{d}x^2} = -q_x, \\ & EJ_z\frac{\mathrm{d}^4v}{\mathrm{d}x^4} + EJ_{yz}\frac{\mathrm{d}^4w}{\mathrm{d}x^4} - \frac{\mathrm{d}}{\mathrm{d}x}\left(N\frac{\mathrm{d}v}{\mathrm{d}x}\right) + \frac{\mathrm{d}^2}{\mathrm{d}x^2}\left(M_y\psi\right) - z_S\frac{\mathrm{d}}{\mathrm{d}x}\left(N\frac{\mathrm{d}\psi}{\mathrm{d}x}\right) + k_y v_R = q_y, \\ & EJ_y\frac{\mathrm{d}^4w}{\mathrm{d}x^4} + EJ_{yz}\frac{\mathrm{d}^4v}{\mathrm{d}x^4} - \frac{\mathrm{d}}{\mathrm{d}x}\left(N\frac{\mathrm{d}w}{\mathrm{d}x}\right) + \frac{\mathrm{d}^2}{\mathrm{d}x^2}\left(M_z\psi\right) + y_S\frac{\mathrm{d}}{\mathrm{d}x}\left(N\frac{\mathrm{d}\psi}{\mathrm{d}x}\right) + k_y v_R = q_z, \\ & EJ_\omega\frac{\mathrm{d}^4\psi}{\mathrm{d}x^4} - GJ_s\frac{\mathrm{d}^2\psi}{\mathrm{d}x^2} - \frac{\mathrm{d}}{\mathrm{d}x}\left[\left(Nr_S^2 - 2\beta_{Sy}M_z + 2\beta_{Sz}M_y + 2\beta_\omega B\right)\frac{\mathrm{d}\psi}{\mathrm{d}x}\right] + M_y\frac{\mathrm{d}^2v}{\mathrm{d}x^2} + M_z\frac{\mathrm{d}^2w}{\mathrm{d}x^2} \\ & \quad - z_S\frac{\mathrm{d}}{\mathrm{d}x}\left(N\frac{\mathrm{d}v}{\mathrm{d}x}\right) + y_S\frac{\mathrm{d}}{\mathrm{d}x}\left(N\frac{\mathrm{d}w}{\mathrm{d}x}\right) - (z_R - z_S)k_y v_R + (y_R - y_S)k_z w_R + k_\psi\psi \\ & \quad == (y_R - y_S)(q_z - q_y\psi) - (z_R - z_S)(q_y + q_z\psi), \end{aligned} \tag{16}$$

In case $q_x = 0$ ($N = \mathrm{const}$), $q_x = 0$ ($N = \mathrm{const}$) and after integrating the first three equations of the above system, we obtain:

$$\begin{aligned} & EA\frac{\mathrm{d}u}{\mathrm{d}x} = N, \\ & EJ_z\frac{\mathrm{d}^2v}{\mathrm{d}x^2} + EJ_{yz}\frac{\mathrm{d}^2w}{\mathrm{d}x^2} - Nv + \left(M_y - z_S N\right)\psi = M_z, \\ & EJ_y\frac{\mathrm{d}^2w}{\mathrm{d}x^2} + EJ_{yz}\frac{\mathrm{d}^2v}{\mathrm{d}x^2} - Nw + (M_z + y_S N)\psi = -M_y, \end{aligned} \tag{17}$$

$$EJ_\omega \frac{\mathrm{d}^4\psi}{\mathrm{d}x^4} - GJ_s \frac{\mathrm{d}^2\psi}{\mathrm{d}x^2} - \frac{\mathrm{d}}{\mathrm{d}x}\left[\left(Nr_S^2 - 2\beta_{Sy}M_z + 2\beta_{Sz}M_y + 2\beta_\omega B\right)\frac{\mathrm{d}\psi}{\mathrm{d}x}\right] + \left(M_y - z_S N\right)\frac{\mathrm{d}^2 v}{\mathrm{d}x^2} + \left(M_z + y_S N\right)\frac{\mathrm{d}^2 w}{\mathrm{d}x^2} == \left(y_Q - y_S\right)\left(q_z - q_y\psi\right) - \left(z_Q - z_S\right)\left(q_y + q_z\psi\right)$$

Global buckling

In the first three loading scenarios, the loss of overall stability, referred to as lateral-torsional buckling, is characterised by the coupled occurrence of twist and out-of-plane bending (Fig. 6), while in the fourth load case the buckling form may be flexural, torsional or flexural-torsional.

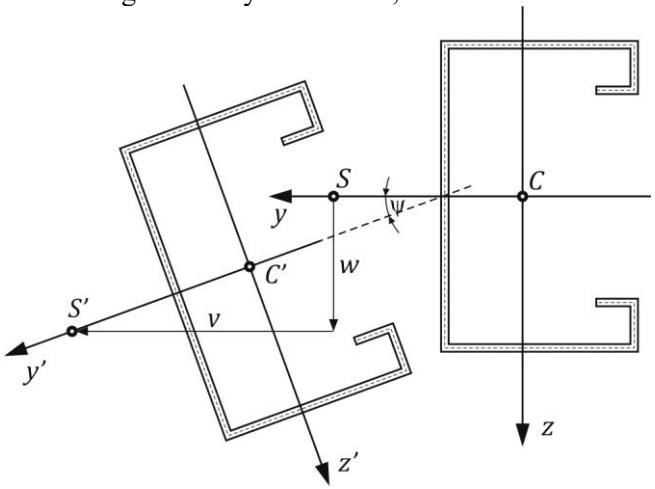

Figure 6. Torsional buckling of a thin-walled beam (28)

Maximum critical moment $M_{max,kr}$ and critical force P_{kr} calculated by solving the system of equations using the Bubnow-Galerkin method, substituting

$$\frac{v}{v_1} = \frac{w}{w_1} = \frac{\psi}{\psi_1} = \sin\frac{\pi x}{L}. \tag{18}$$

In the first three load cases the critical maximum moment $M_{max,kr}$ was

$$M_{max,kr} = C_1\left(\frac{\pi}{L}\right)^2 E\frac{J_yJ_z - J_{yz}^2}{J_y}\left\{C_2\left(z_Q - z_S\right) + C_3\beta_{Sz} \pm \sqrt{\left[C_2\left(z_Q - z_S\right) + C_3\beta_{Sz}\right]^2 + \frac{J_yJ_\omega}{J_yJ_z - J_{yz}^2}\left[1 + \frac{GJ_s}{EJ_\omega}\left(\frac{L}{\pi}\right)^2\right]}\right\}. \tag{19}$$

The constants C_i for $i = 1,2,3$, depending on the load, took the following values:

- in the load case I

$$C_1 = 1, \quad C_2 = 0, \quad C_3 = 1, \tag{20}$$

- in the load case II

$$C_1 = \frac{\pi^2}{2}\sqrt{\frac{15}{2(\pi^4+45)}} = 1.1325, \qquad C_2 = \sqrt{\frac{30}{\pi^4+45}} = 0.4590, \qquad C_3 = (\pi^2-3)\sqrt{\frac{5}{6(\pi^4+45)}} = 0{,}5255, \tag{21}$$

- in the load case III

$$C_1 = \pi\sqrt{\frac{3}{\pi^2+6}} = 1.3659 \qquad C_2 = \frac{4}{\pi}\sqrt{\frac{3}{\pi^2+6}} = 0.5536, \tag{22}$$

$$C_3 = \frac{\pi^2 - 4}{2\pi}\sqrt{\frac{3}{\pi^2 + 6}} = 0.4062.$$

In the IV load case, the critical force is the smallest eigenvalue of the equation

$$A - PB = 0, \tag{23}$$

where

$$A = \begin{bmatrix} P_z & P_{yz} & 0 \\ P_{yz} & P_y & 0 \\ 0 & 0 & r_S^2 P_\psi \end{bmatrix}, \qquad B = \begin{bmatrix} 1 & 0 & z_S \\ 0 & 1 & -y_S \\ z_S & -y_S & r_S^2 \end{bmatrix} \tag{24}$$

and

$$P_y = \left(\frac{\pi}{L}\right)^2 EJ_y, \quad P_{yz} = \left(\frac{\pi}{L}\right)^2 EJ_{yz}, \quad P_z = \left(\frac{\pi}{L}\right)^2 EJ_z, \quad P_\psi = \frac{1}{r_S^2}\left(\frac{\pi}{L}\right)^2 EJ_\omega \left[1 + \frac{GJ_S}{EJ_\omega}\left(\frac{L}{\pi}\right)^2\right] \tag{25}$$

Distortional buckling

Beam instability may also manifest through flange buckling accompanied by concurrent deformation of the web. This type of buckling is called distortional buckling. In a simplified model of this form of buckling, the beam flange is treated as a beam elastically supported at the edge of its connection to the web (Figure). Such a model can be found in Hancock (31), Schafer and Perköz (32), Teng et al. (33) and Pawlak et al. (28).

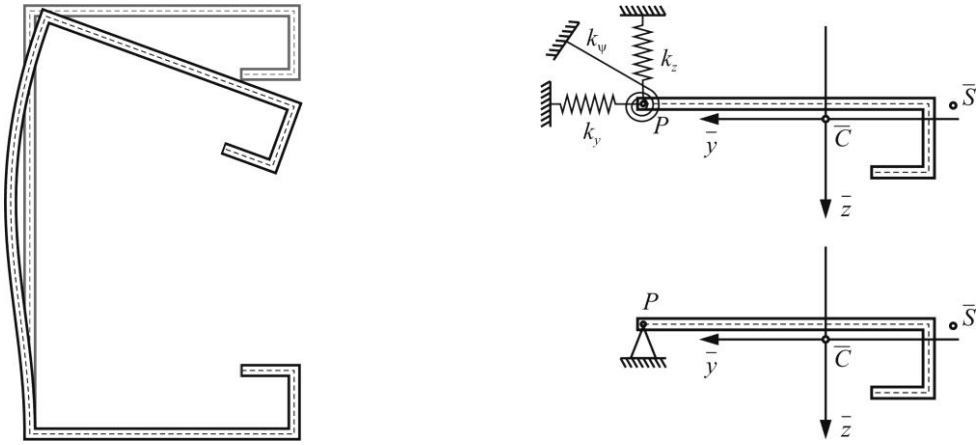

Figure 7. Flange buckling (28)

The stresses in the beam can be represented by the formula

$$\sigma_x(x, \bar{y}, \bar{z}) = \frac{N}{A} + \frac{(\bar{z} - \bar{z}_C)J_z - (\bar{y} - \bar{y}_C)J_{yz}}{J_y J_z - J_{yz}^2} M_y, \tag{26}$$

where $(x, \bar{y}, \bar{z})$ denotes the centroidal coordinate system associated with the beam flange. The geometric properties of the flange cross-section are indicated similarly to those of the entire beam cross-section by adding a single overline.

The internal forces occurring in the flange are

$$\bar{N} = \int_{\bar{A}} \sigma_x d\bar{A} = \left(\frac{N}{A} - \frac{\bar{z}_C J_z - \bar{y}_C J_{yz}}{J_y J_z - J_{yz}^2} M_y\right)\bar{A}, \tag{27}$$

$$\bar{M}_{\bar{y}} = \int_{\bar{A}} \bar{z}\sigma_x d\bar{A} = \frac{\bar{J}_{\bar{y}} J_z - \bar{J}_{\bar{y}\bar{z}} J_{yz}}{J_y J_z - J_{yz}^2} M_y, \tag{28}$$

$$\bar{M}_{\bar{z}} = -\int_{\bar{A}} \bar{y}\sigma_x d\bar{A} = -\frac{\bar{J}_{\bar{y}\bar{z}} J_z - \bar{J}_{\bar{z}} J_{yz}}{J_y J_z - J_{yz}^2} M_y, \tag{29}$$

$$\bar{B} = -\int_{\bar{A}} \bar{\omega}\sigma_x d\bar{A} = 0. \tag{30}$$

After simplification $\bar{v}_P = 0$, $\bar{w}_P = 0$ i $k_\psi = 0$ the displacements of the beam flange are

$$\bar{v} = (\bar{z}_P - \bar{z}_{\bar{S}})\bar{\psi}, \tag{31}$$

$$\bar{w} = -(\bar{y}_P - \bar{y}_{\bar{S}})\bar{\psi}. \tag{32}$$

The elastic deformation energy of the beam flange after introducing the internal forces into equation (12) is equal to

$$U_{\varepsilon l} = \frac{1}{2}E\bar{J}_{\bar{\omega}_P}\int_0^L \left(\frac{\mathrm{d}^2\bar{\psi}}{\mathrm{d}x^2}\right)^2 \mathrm{d}x + \frac{1}{2}G\bar{J}_s\int_0^L \left(\frac{\mathrm{d}\bar{\psi}}{\mathrm{d}x}\right)^2 \mathrm{d}x, \tag{33}$$

$$\begin{aligned} U_{\varepsilon n} = \frac{1}{2}\int_0^L \left[\bar{r}_P^2\bar{N} + 2\bar{\beta}_{P\bar{z}}\bar{M}_{\bar{y}} - 2\bar{\beta}_{P\bar{y}}\bar{M}_{\bar{z}}\right]\left(\frac{\mathrm{d}\bar{\psi}}{\mathrm{d}x}\right)^2 \mathrm{d}x + \\ + \frac{1}{2}\int_0^L \left[(\bar{z}_P - \bar{z}_{\bar{S}})\frac{\mathrm{d}^2\bar{M}_{\bar{y}}}{\mathrm{d}x^2} - (\bar{y}_P - \bar{y}_{\bar{S}})\frac{\mathrm{d}^2\bar{M}_{\bar{z}}}{\mathrm{d}x^2}\right]\bar{\psi}^2 \mathrm{d}x \end{aligned} \tag{34}$$

where

$$\begin{gathered} \bar{r}_P^2 = \frac{\bar{J}_{\bar{y}} + \bar{J}_{\bar{z}}}{\bar{A}} + \bar{y}_P^2 + \bar{z}_P^2, \\ \bar{J}_{\bar{\omega}_P} = \bar{J}_{\bar{\omega}} + (\bar{y}_P - \bar{y}_{\bar{S}})^2\bar{J}_{\bar{y}} - 2(\bar{y}_P - \bar{y}_{\bar{S}})(\bar{z}_P - \bar{z}_{\bar{S}})\bar{J}_{\bar{y}\bar{z}} + (\bar{z}_P - \bar{z}_{\bar{S}})^2\bar{J}_{\bar{z}}, \\ \bar{\beta}_{P\bar{y}} = \bar{\beta}_{\bar{S}\bar{y}} + \bar{y}_{\bar{S}} - \bar{y}_P, \qquad \bar{\beta}_{P\bar{z}} = \bar{\beta}_{\bar{S}\bar{z}} + \bar{z}_{\bar{S}} - \bar{z}_P, \end{gathered} \tag{35}$$

The nonlinear part of the elastic deformation energy can be written as

$$U_{\varepsilon n} = \frac{1}{2}J_N\int_0^L N\left(\frac{\mathrm{d}\bar{\psi}}{\mathrm{d}x}\right)^2 \mathrm{d}x - \frac{1}{2}J_{M1}\int_0^L M_y\left(\frac{\mathrm{d}\bar{\psi}}{\mathrm{d}x}\right)^2 \mathrm{d}x + \frac{1}{2}J_{M2}\int_0^L \frac{\mathrm{d}^2M_y}{\mathrm{d}x^2}\bar{\psi}^2 \mathrm{d}x, \tag{36}$$

where

$$\begin{gathered} J_N = \bar{r}_P^2\frac{\bar{A}}{A}, \\ J_{M1} = \frac{\left(\bar{z}_C\bar{r}_P^2\bar{A} - 2\bar{\beta}_{P\bar{z}}\bar{J}_{\bar{y}} - 2\bar{\beta}_{P\bar{y}}\bar{J}_{\bar{y}\bar{z}}\right)J_z - \left(\bar{y}_C\bar{r}_P^2\bar{A} - 2\bar{\beta}_{P\bar{z}}\bar{J}_{\bar{y}\bar{z}} - 2\bar{\beta}_{P\bar{y}}\bar{J}_{\bar{z}}\right)J_{yz}}{J_yJ_z - J_{yz}^2}, \\ J_{M2} = \frac{\left[(\bar{z}_P - \bar{z}_{\bar{S}})\bar{J}_{\bar{y}} + (\bar{y}_P - \bar{y}_{\bar{S}})\bar{J}_{\bar{y}\bar{z}}\right]J_z - \left[(\bar{z}_P - \bar{z}_{\bar{S}})\bar{J}_{\bar{y}\bar{z}} + (\bar{y}_P - \bar{y}_{\bar{S}})\bar{J}_{\bar{z}}\right]J_{yz}}{J_yJ_z - J_{yz}^2}. \end{gathered} \tag{37}$$

The critical loads were calculated using the Ritz method from the equation

$$\delta(U_\varepsilon) = 0. \tag{38}$$

Assuming the shelf rotation angle in the form

$$\bar{\psi}(x) = \sum_{m=1}^{\infty} \psi_m \sin\frac{m\pi x}{L} \tag{39}$$

The equation is obtained in the form

$$\det(K_L - M_{max}K_G) = 0 \qquad \text{lub} \qquad \det(K_L - PK_G) = 0. \tag{40}$$

Matrice K_L for all load cases is:

$$[K_L]_{mk} = \frac{\pi^2}{2L} \times \begin{cases} m^2\left[G\bar{J}_s + m^2\left(\frac{\pi}{L}\right)^2 E\bar{J}_{\bar{\omega}_P}\right] & \text{for} \quad m = k, \\ 0 & \text{for} \quad m \neq k \end{cases} \tag{41}$$

Matrices K_G are respectively equal:

- in the load case I

$$[K_G]_{mk} = \frac{\pi^2}{2L} \times \begin{cases} m^2 J_{M1} & \text{for} \quad m = k \\ 0 & \text{for} \quad m \neq k \end{cases}, \tag{42}$$

- in the load case II

$$[K_G]_{mk} = \frac{\pi^2}{2L} \times \begin{cases} \frac{2}{3} m^2 J_{M1} - \frac{2}{\pi^2}(J_{M1} - 4J_{M2}) & \text{for} \quad m = k \\ -\frac{8}{\pi^2} mk \frac{m^2 + k^2}{(m^2 - k^2)^2} [1 + (-1)^{m+k}] J_{M1} & \text{for} \quad m \neq k \end{cases}, \tag{43}$$

- in the load case III

$$[K_G]_{mm} = \frac{\pi^2}{2L}\left[\frac{1}{2} m^2 J_{M1} - \frac{1 - (-1)^m}{\pi^2}(J_{M1} - 4J_{M2})\right], \tag{44}$$

$$[K_G]_{mk} = -\frac{\pi^2}{2L}\frac{4}{\pi^2}\left\{\frac{mk}{(m^2 - k^2)^2}\left[(m^2 + k^2)\left(1 + (-1)^{m+k}\right) - (m + k)^2 \cos\frac{(m - k)\pi}{2}\right.\right.$$
$$\left.\left. - (m - k)^2 \cos\frac{(m + k)\pi}{2}\right] J_{M1} - \left[\cos\frac{(m - k)\pi}{2} - \cos\frac{(m + k)\pi}{2}\right] J_{M2}\right\}, \tag{45}$$

If a diaphragm occurs in the middle of the beam length, the number of buckling half-waves along the beam length can only be an even number. Therefore, the flange rotation angle is approximated by

$$\bar{\psi}(x) = \sum_{m=1}^{\infty} \psi_m \sin\frac{2m\pi x}{L} \tag{46}$$

then

$$[K_L]_{mk} = \frac{\pi^2}{2L} \times \begin{cases} 4m^2\left[G\bar{J}_s + 4m^2\left(\frac{\pi}{L}\right)^2 E\bar{J}_{\bar{\omega}_P}\right] & \text{for} \quad m = k \\ 0 & \text{for} \quad m \neq k \end{cases}, \tag{47}$$

$$[K_G]_{mk} = \frac{\pi^2}{2L} \times \begin{cases} 2m^2 J_{M1} & \text{for} \quad m = k \\ -\frac{8}{\pi^2} mk \frac{m^2 + k^2}{(m^2 - k^2)^2} [1 - (-1)^{m+k}] J_{M1} & \text{for} \quad m \neq k \end{cases}, \tag{48}$$

- in the load case III

$$[K_G]_{mk} = \frac{\pi^2}{2L} \times \begin{cases} m^2 J_N & \text{for} \quad m = k \\ 0 & \text{for} \quad m \neq k \end{cases}, \tag{49}$$

In load cases I and IV, the formulas for the critical load can be presented explicitly

$$M_{max,kr} = \frac{G\bar{J}_s + E\bar{J}_{\bar{\omega}_P}\left(\frac{\pi}{L}\right)^2}{J_{M1}}, \tag{50}$$

$$P_{kr} = \frac{G\bar{J}_s + E\bar{J}_{\bar{\omega}_P}\left(\frac{\pi}{L}\right)^2}{J_N}. \tag{51}$$

Local buckling

Loss of local stability manifests itself as buckling of individual beam walls. In this study, a simplified buckling model was adopted, treating the individual beam walls as plates with length L, width h and thickness t, which are:

- supported on four edges – span walls (Figure),

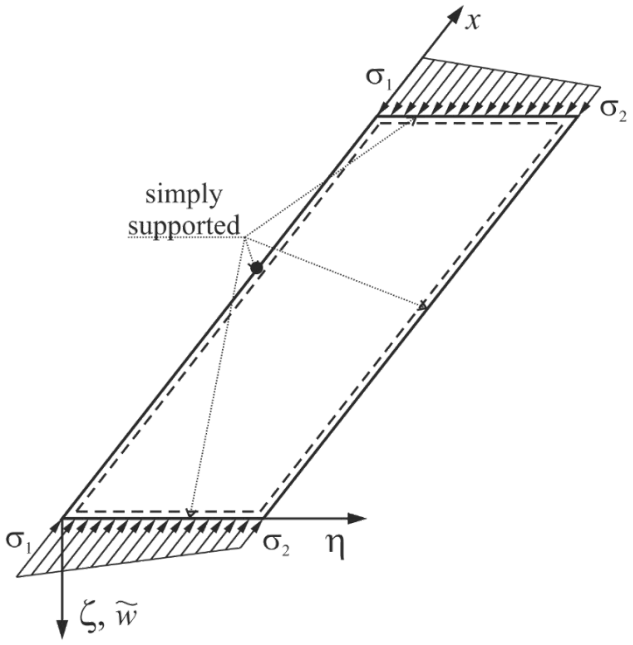

Figure 8. Span wall model (28)

- supported on three edges and with one free edge - cantilever walls (Figure).

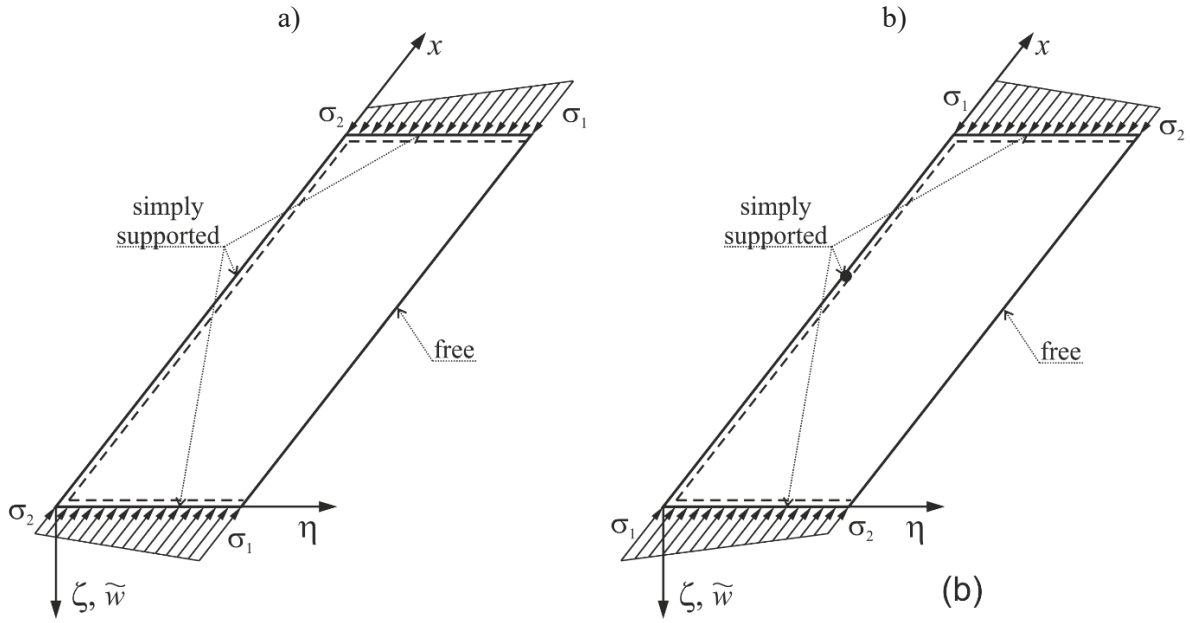

Figure 9. Cantilever wall models (28)

A local reference coordinate system was established for the beam wall under consideration, as shown in Figure and Figure . The elastic strain potential energy for the plate can be represented as:

$$U_\varepsilon = U_{\varepsilon l} + U_{\varepsilon n}, \tag{52}$$

where:

$$U_{\varepsilon l} = \frac{1}{2} D \int_0^L \int_0^h \left\{ \left(\frac{\partial^2 \widetilde{w}}{\partial x^2} + \frac{\partial^2 \widetilde{w}}{\partial \eta^2} \right)^2 - 2(1-v) \left[\frac{\partial^2 \widetilde{w}}{\partial x^2} \frac{\partial^2 \widetilde{w}}{\partial \eta^2} - \left(\frac{\partial^2 \widetilde{w}}{\partial x \partial \eta} \right)^2 \right] \right\} \mathrm{d}\eta \mathrm{d}x \tag{53}$$

$$U_{\varepsilon n} = \frac{1}{2} t \int_0^L \int_0^h \sigma_x \left(\frac{\partial \widetilde{w}}{\partial x} \right)^2 \mathrm{d}\eta \mathrm{d}x \tag{54}$$

The stresses are equal to

$$\sigma_x(x,\eta) = -\frac{P}{A} + \frac{z(\eta)J_z - y(\eta)J_{yz}}{J_yJ_z - J_{yz}^2}M_y(x), \tag{55}$$

Let σ_1 denote the greatest compressive stress, and σ_2 the stress occurring in the middle of the length of the opposite edge and let $\psi = \frac{\sigma_2}{\sigma_1}$, then in the case of span and cantilever walls, in which the maximum compressive stresses occur on the pin-supported edge, the following relations apply (Figure , Figure b):

$$\sigma_1 = -\sigma_x\left(\frac{L}{2}, 0\right), \qquad \sigma_2 = -\sigma_x\left(\frac{L}{2}, h\right). \tag{56}$$

In the case of cantilever walls, where the maximum compressive stresses occur at the free edge (Figure a):

$$\sigma_1 = -\sigma_x\left(\frac{L}{2}, h\right), \qquad \sigma_2 = -\sigma_x\left(\frac{L}{2}, 0\right). \tag{57}$$

To summarize the stresses:

$$\sigma_x(x,\eta) = -f_M(x)g_M(\eta)\sigma_1 = -\kappa\frac{\pi^2 D}{th}f_M(x)g_M(\eta), \tag{58}$$

where κ is the local instability parameter.
Function $f(x)$ depends on the load case and is equal to:

- in the load case I and IV

$$f_M(x) = 1, \tag{59}$$

- in the load case II

$$f_M(x) = 4\frac{x}{L}\left(1 - \frac{x}{L}\right) \tag{60}$$

- in the load case III

$$f_M(x) = \begin{cases} 2\dfrac{x}{L} & \text{dla} \quad 0 \le x \le \dfrac{L}{2} \\ 2\left(1 - \dfrac{x}{L}\right) & \text{dla} \quad \dfrac{L}{2} < x \le L \end{cases}, \tag{61}$$

However, the function $g_M(\eta)$ equals

$$g_M(\eta) = (1-\psi)\frac{\eta}{h} + \psi, \qquad \text{when} \quad \sigma_1 = -\sigma_x\left(\tfrac{L}{2}, h\right), \qquad \text{then} \quad \eta_1 = h \tag{62}$$

or

$$g_M(\eta) = (\psi - 1)\frac{\eta}{h} + 1, \qquad \text{when} \quad \sigma_1 = -\sigma_x\left(\tfrac{L}{2}, 0\right), \qquad \text{then} \quad \eta_1 = 0. \tag{63}$$

The maximum critical moment can be calculated from the formula

$$M_{max,cr} = \sigma_{1,cr}\frac{J_yJ_z - J_{yz}^2}{z_1J_z - y_1J_{yz}} = \kappa_{cr}\frac{\pi^2 D}{th}\frac{J_yJ_z - J_{yz}^2}{z_1J_z - y_1J_{yz}}, \tag{64}$$

where $y_1 = y(\eta_1)$ i $z_1 = z(\eta_1)$.
However, the critical force is equal to

$$P_{max,cr} = \sigma_{1,cr}A = \kappa_{cr}\frac{\pi^2 D}{th}A, \tag{65}$$

The critical stresses were calculated using the Ritz method based on the principle of minimum total potential energy

$$\delta(U_\varepsilon) = 0. \tag{66}$$

For span walls, the deflection was approximated by the series

$$\widetilde{w} = \sum_{m=1}^{\infty}\sum_{n=1}^{\infty} w_{mn}\sin\frac{m\pi x}{L}\cos\frac{n\pi\eta}{h} \tag{67}$$

Limiting to a few dozen terms, i.e. $m = 1, \dots, M$, $n = 1, \dots, N$.
Potential energy can be represented in matrix form

$$U_{\varepsilon l} = \frac{1}{2}\widetilde{w}^T K_L \widetilde{w}, \qquad U_{\varepsilon n} = -\frac{1}{2}\kappa\widetilde{w}^T K_G \widetilde{w}, \tag{68}$$

where

$$\widetilde{w}^T = [w_{11}, w_{21}, \dots, w_{M1}, w_{12}, \dots, w_{MN}] \tag{69}$$

and

$$[K_L]_{ij} = D\frac{\pi^4}{4Lh}\left\{\frac{1}{\lambda^2}U_{mk}^{22}V_{nl}^{00} + 2U_{mk}^{20}V_{nl}^{02} + \lambda^2 U_{mk}^{00}V_{nl}^{22} - 2(1-v)\left[U_{mk}^{20}V_{nl}^{02} - U_{mk}^{11}V_{nl}^{11}\right]\right\}$$

$$[K_G]_{ij} = D\frac{\pi^4}{4Lh}\widehat{U}_{mk}^{11}\widehat{V}_{nl}^{00}$$

$$\text{for } i = (n-1)M + m,\ \ j = (k-1)M + l$$

$$U_{mk}^{rs} = \frac{2}{L}\left(\frac{L}{\pi}\right)^{r+s}\int_0^L \frac{\mathrm{d}^r}{\mathrm{d}x^r}\left(\sin\frac{m\pi x}{L}\right)\frac{\mathrm{d}^s}{\mathrm{d}x^s}\left(\sin\frac{k\pi x}{L}\right)\mathrm{d}x$$

$$V_{nl}^{rs} = \frac{2}{h}\left(\frac{h}{\pi}\right)^{r+s}\int_0^h \frac{\mathrm{d}^r}{\mathrm{d}y^r}\left(\sin\frac{n\pi y}{h}\right)\frac{\mathrm{d}^s}{\mathrm{d}y^s}\left(\sin\frac{l\pi y}{h}\right)\mathrm{d}y \tag{70}$$

$$\widehat{U}_{mk}^{rs} = \frac{2}{L}\left(\frac{L}{\pi}\right)^{r+s}\int_0^L f_M(x)\frac{\mathrm{d}^r}{\mathrm{d}x^r}\left(\sin\frac{m\pi x}{L}\right)\frac{\mathrm{d}^s}{\mathrm{d}x^s}\left(\sin\frac{k\pi x}{L}\right)\mathrm{d}x$$

$$\widehat{V}_{nl}^{rs} = \frac{2}{h}\left(\frac{h}{\pi}\right)^{r+s}\int_0^h g_M(y)\frac{\mathrm{d}^r}{\mathrm{d}y^r}\left(\sin\frac{n\pi y}{h}\right)\frac{\mathrm{d}^s}{\mathrm{d}y^s}\left(\sin\frac{l\pi y}{h}\right)\mathrm{d}y$$

Matrice K_L can be written in the form

$$[K_L]_{ij} = D\frac{\pi^4}{4Lh}\begin{cases}\left(\frac{m^2}{\lambda} + n^2\lambda\right)^2 & \text{dla } \ m = k \ \wedge \ n = l \\ 0 & \text{dla } \ m \neq k \ \vee n \neq l\end{cases} \tag{71}$$

However, the integrals $\widehat{U}_{mk}^{11}$ are equal:

- in the load case I and IV

$$\widehat{U}_{mk}^{11} = \begin{cases} m^2 & \text{for } \ m = k \\ 0 & \text{for } \ m \neq k \end{cases}, \tag{72}$$

- in the load case II

$$\widehat{U}_{mk}^{11} = \begin{cases} \frac{2}{3\pi^2}(m^2\pi^2 - 3) & \text{for } \ m = k \\ -\frac{8}{\pi^2}mk\frac{m^2 + k^2}{(m^2 - k^2)^2}[1 + (-1)^{m+k}] & \text{for } \ m \neq k \end{cases}, \tag{73}$$

- in the load case III

$$\widehat{U}_{mk}^{11} = \begin{cases} \frac{1}{2\pi^2}(m^2\pi^2 - 1 + (-1)^m) & \text{fo} \\ -\frac{4}{\pi^2}mk\frac{(m^2 + k^2)\left(1 + (-1)^{m+k}\right) - (m+k)^2\cos\frac{(m-k)\pi}{2} - (m-k)^2\cos\frac{(m+k)\pi}{2}}{(m^2 - k^2)^2} & \text{fo} \end{cases} \quad ($$

If we consider the diaphragm at the middle of the beam length

$$\widehat{U}_{mk}^{11} = \begin{cases} \frac{m^2}{2} & \text{for } \ m = k \ \wedge m, k \text{ - even} \\ -\frac{8}{\pi^2}mk\frac{(m^2 + k^2)}{(m^2 - k^2)^2}\left(1 - (-1)^{\frac{m+k}{2}}\right) & \text{for } \ m \neq k \wedge m, k \text{ - even} \\ 0 & m, k \text{ - odd} \end{cases} \tag{75}$$

or when we substitute

$$\widetilde{w} = \sum_{m=1}^{\infty}\sum_{n=1}^{\infty} w_{mn}\sin\frac{2m\pi x}{L}\cos\frac{n\pi\eta}{h} \tag{76}$$

then

$$[K_L]_{ij} = D\frac{\pi^4}{4Lh}\begin{cases}\left(4\frac{m^2}{\lambda}+n^2\lambda\right)^2 & \text{for } m=k \ \wedge \ n=l \\ 0 & \text{for } m\neq k \ \vee n\neq l\end{cases} \tag{77}$$

$$\widehat{U}_{mk}^{11} = \begin{cases} 2m^2 & \text{for } m=k \\ -\frac{8}{\pi^2}mk\frac{(m^2+k^2)}{(m^2-k^2)^2}\left(1-(-1)^{m+k}\right) & \text{for } m\neq k\end{cases} \tag{78}$$

The integral $\widehat{V}_{nl}^{00}$ is

$$\widehat{V}_{nl}^{00} = \begin{cases} \frac{1}{2}(1+\psi) & \text{for } n=l \\ \frac{4}{\pi^2}\frac{nl}{(n^2-l^2)^2}[1-(-1)^{n+l}](1-\psi) & \text{for } n\neq l\end{cases}. \tag{79}$$

The critical values of the local instability parameter κ for the span walls and for selected values of the boundary stress ratio ψ are presented in the graphs (Figure – 12).

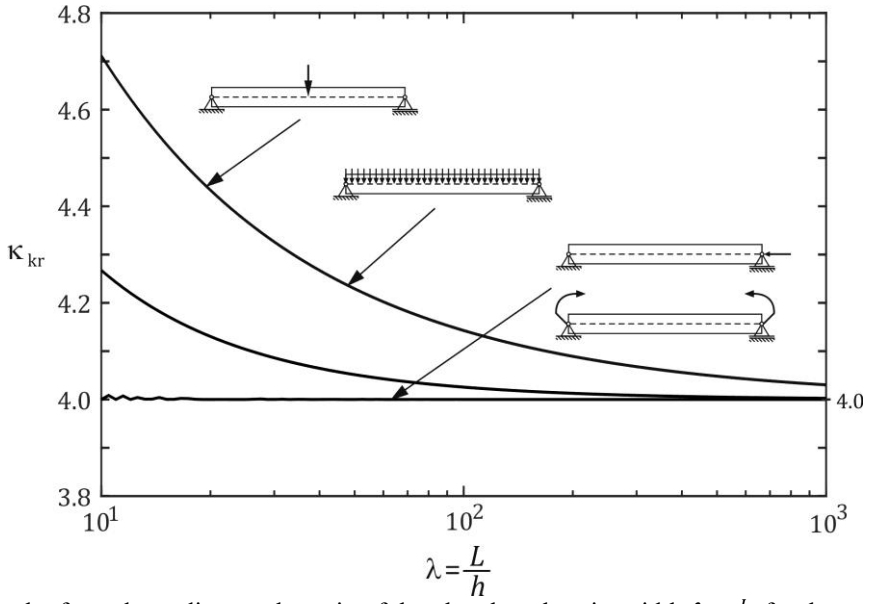

Figure 10. Graph of κ_{kr} depending on the ratio of the plate length to its width $\lambda = \frac{L}{h}$ for the parameter $\psi = 1$ (span walls)

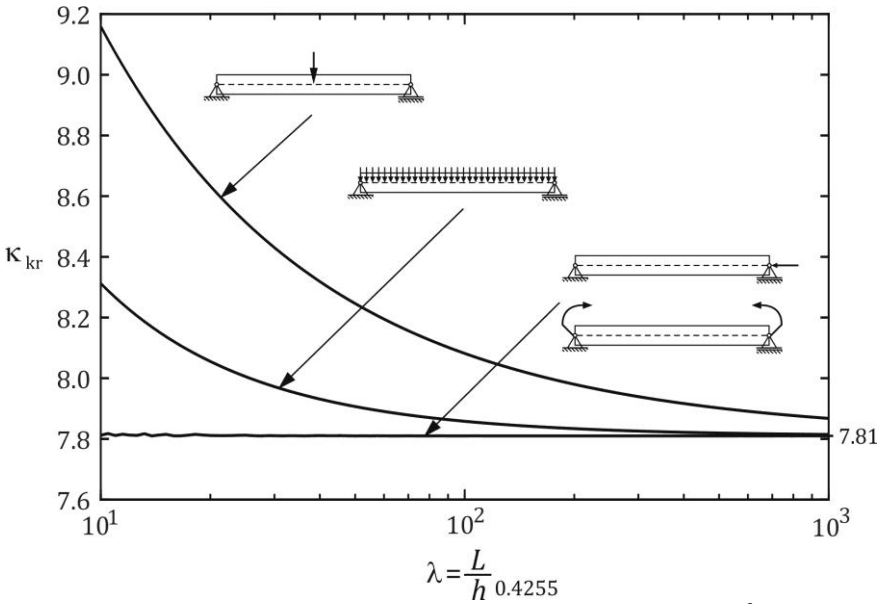

Figure 11. Graph of κ_{kr} depending on the ratio of the plate length to its width $\lambda = \frac{L}{h}$ for the parameter $\psi = 0$ (span walls)

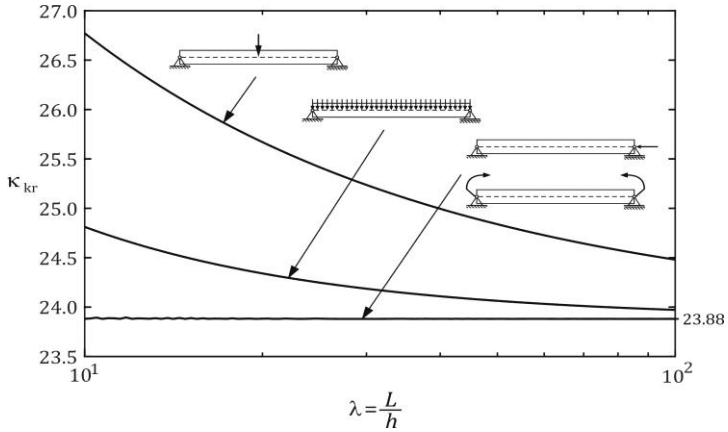

Figure 12. Graph of κ_{kr} depending on the ratio of the plate length to its width $\lambda = \frac{L}{h}$ for the parameter $\psi = -1$ (span walls)

For cantilever walls, the deflection was approximated by the series

$$\widetilde{w} = \sum_{m=1}^{\infty} w_m \frac{\eta}{h} \sin\frac{m\pi x}{L} \tag{80}$$

By limiting to a finite number of ingredients, i.e. $m = 1, \ldots, M$.
Similarly to the case of span walls, the potential energy can be presented in the matrix form, where

$$\widetilde{w}^T = [w_1, w_2, \ldots, w_M] \tag{81}$$

and

$$\begin{aligned} [K_L]_{mk} &= D\frac{\pi^4}{4Lh}\begin{cases}\frac{2}{3}m^2\left(\frac{6}{\pi^2}(1-v)+\frac{m^2}{\lambda^2}\right) & \text{for } m = k,\\ 0 & \text{for } m \neq k\end{cases}\\ [K_G]_{mk} &= D\frac{\pi^4}{4Lh}\left(\frac{1}{2}+\frac{1}{6}\psi\right)\widehat{U}_{mk}^{11} \text{ for } \eta_1 = h,\\ [K_G]_{mk} &= D\frac{\pi^4}{4Lh}\left(\frac{1}{6}+\frac{1}{2}\psi\right)\widehat{U}_{mk}^{11} \text{ for } \eta_1 = 0. \end{aligned} \tag{82}$$

The critical values of the local instability parameter κ for cantilever walls and for a boundary stress ratio of $\psi = 1$ are shown in the graph (Figure 13).

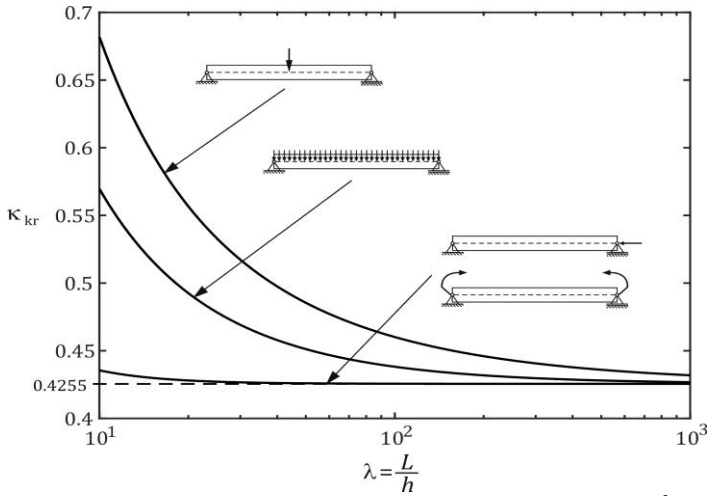

Figure 13. Graph of κ_{kr} depending on the ratio of the plate length to its width $\lambda = \frac{L}{h}$ for the parameter $\psi = 1$ (cantilever walls)

The critical values of the parameter κ for other values of the boundary stress ratio ψ can be calculated as follows:

$$\kappa_{kr} = \frac{4}{3+\psi}\kappa_{kr,\psi=1} \quad \text{for} \quad \eta_1 = h \tag{83}$$

or

$$\kappa_{kr} = \frac{4}{1+3\psi}\kappa_{kr,\psi=1} \quad \text{for} \quad \eta_1 = 0. \tag{84}$$

ANALYTICAL SOLUTIONS RESULTS

The analytical results reported in this chapter were generated using a dedicated computational tool implementing the formulations described herein. The program, referred to as GUI, was developed in MATLAB and authored by Marcin Rodak (34). This section presents the results obtained for double-bend C-sections and Z-sections. The C-sections were bent in two planes as shown in Figure 14 and named C1 and C2, respectively. The Z-sections were bent in the planes shown in Figure 14. The critical loads in bending were obtained for beams with a length of $L = 420$ mm, and in compression, $L = 800$ mm.

Results were obtained for the following material constants for Steel DC01:

- Young's modulus – $E = 2.0 \cdot 10^5$ MPa,
- Kirchhoff's modulus – $G = E/(2(1+\nu)) = 7.6923 \cdot 10^4$ MPa,
- Poisson's ratio – $\nu = 0.3$.

Table 1 presents the results obtained for channel C1. The lowest critical load values for bending were obtained for the local mode of stability loss (web buckling) (Figure 15). Using the finite strip method (FSM), the critical moment value for pure bending was $M_{max,kr} = 0.6298$ kNm, and the number of buckling half-waves along the beam length was 9 (buckling half-wave length 46.67 mm). Buckling occurred through local stability loss (Figure 16). The nearly 30% lower critical load values presented in Table 1 result from a simplified model of local stability loss, where the flange walls were treated as non-cooperating plates.

In the compression case, the lowest critical load was obtained for distortional buckling of the flange. This result is significantly lower than the FSM result. This is a consequence of the simplified distortional buckling model, which does not take into account the effect of the stiffness of the web and the rest of the profile on the critical load required for flange buckling. In the finite strip method, the lowest critical force was obtained for local buckling (Figure 18) with a value of $P_{kr} = 50.73$ kN (the number of buckling half-waves along the beam length was 17, and the buckling half-wave length was 47.06 mm). The error between the critical forces obtained by the two methods was also approximately 30%.

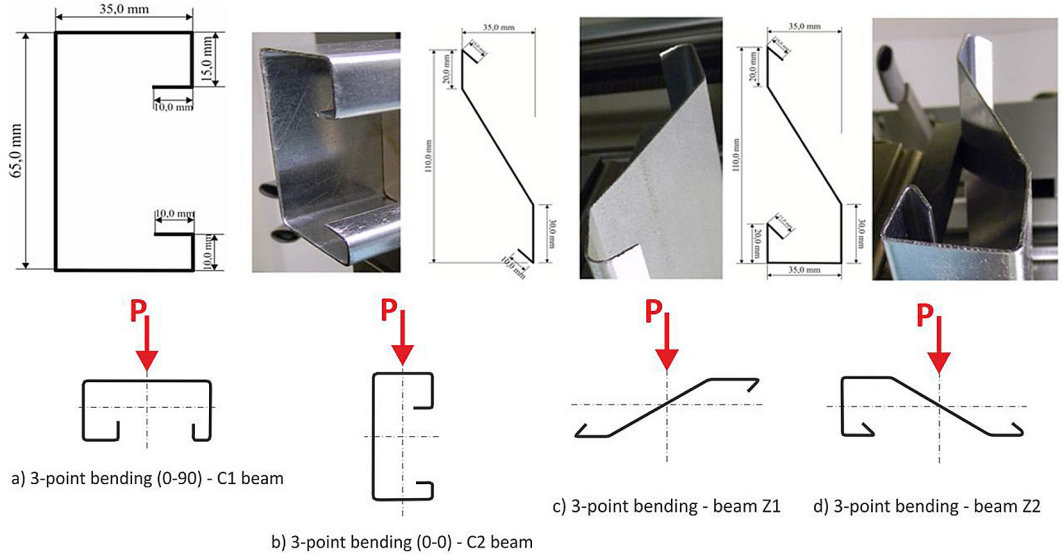

Figure 14. Tested cross-sections and load plane

Table 1. Critical loads for profile C1. In load cases I, II, III the beam length was L = 420 mm, in case IV L = 800 mm

Buckling form	Load case					
	I	II		III		IV
	$M_{max,kr}$ [kNm]	$M_{max,kr}$ [kNm]	q_{kr} [kN/m]	$M_{max,kr}$ [kNm]	F_{kr} [kN]	P_{kr} [kN]
Global	99.52	67.22	3049	68.44	65.19	59.611
Distortional	-	-	-	-	-	7.4599
Local	0.4509 (web)	0.4940 (web)	22.40 (web)	0.5538 (web)	5.274 (web)	37.219 (web)

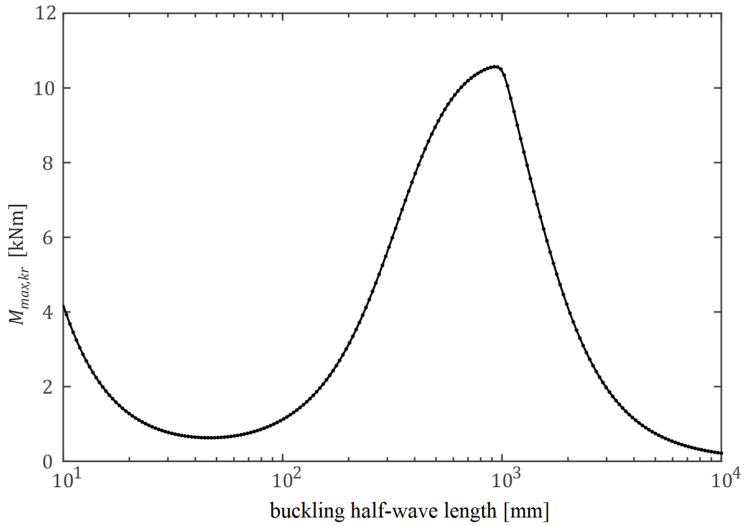

Figure 15. The critical moment diagram obtained using the finite strip method for profile C1 in load case I

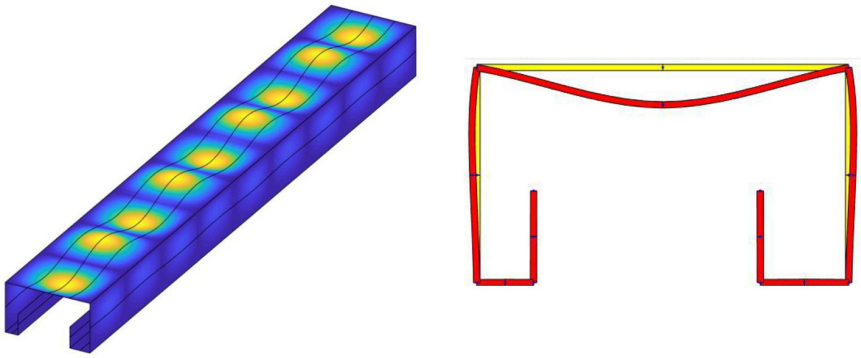

Figure 16. Buckling shape obtained using the finite strip method (profile C1, load case I)

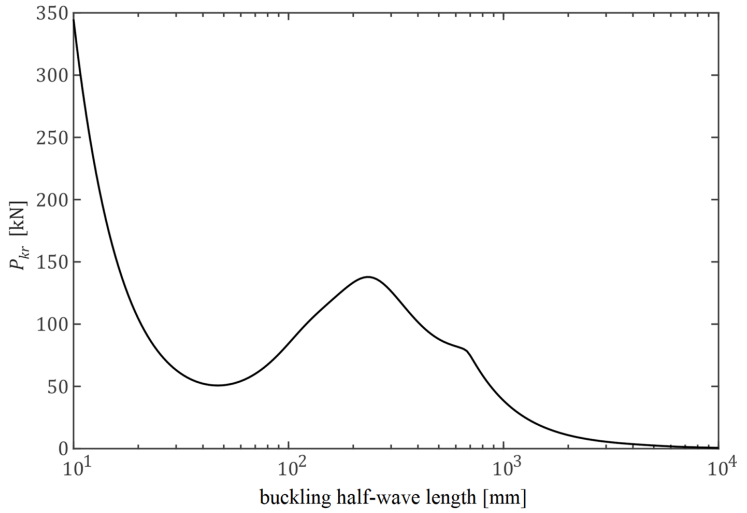

Figure 17. The critical force diagram obtained by the finite strip method for the C1 profile in the IV load case

Figure 15 and Figure 17 presents the graphs of the critical moment $M_{max,kr}$ in the load case I and the critical force in the load case IV, depending on the length of the buckling half-wave for the C1 profile, respectively.

Table 2 presents the results obtained for channel C2. Similarly to the bent channel C1, the lowest critical load value was obtained for the local mode of stability loss, but through buckling of the flange. In the finite strip method, the critical moment value

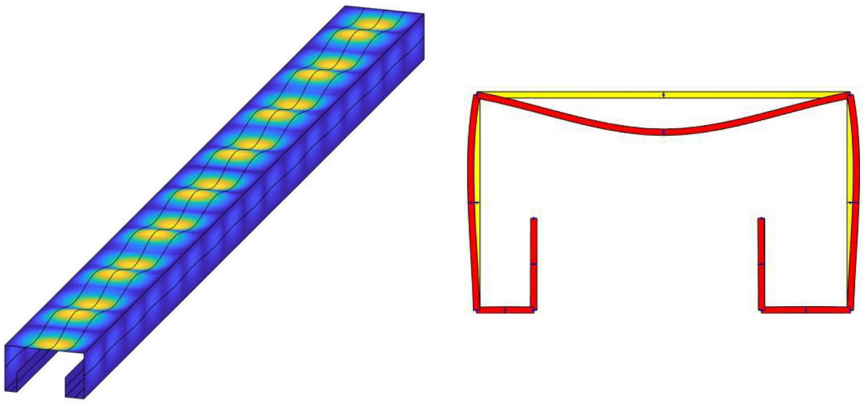

Figure 18. Buckling shape obtained using the finite strip method (profile C1, load case IV)

Table 2. Critical loads for profile C2. In load cases I, II, III the beam length was L = 420 mm, in case IV L = 800 mm

Buckling form	Load case					
	I	II		III		IV
	$M_{max,kr}$ [kNm]	$M_{max,kr}$ [kNm]	q_{kr} [kN/m]	$M_{max,kr}$ [kNm]	F_{kr} [kN]	P_{kr} [kN]
Global	16.05	17.18	779.0	20.43	194.6	59.61
Distortional	5.288	12.80	580.6	38.84	369.9	7.460
Local	2.108 (flange)	2.219 (flange)	100.6 (flange)	2.428 (flange)	23.12 (flange)	37.22 (web)

$M_{max,kr}$ = 2.817 kNm was obtained (Figure 18, 19) (the number of buckling half-waves along the beam length was 15, and the buckling half-wave length was 28 mm), and buckling also occurred through local stability loss of the flange (Figure 20).

Table 3 presents the results obtained for the Z1-section. In bending, the lowest critical load value was obtained for the local mode of stability loss (web buckling). Using the finite strip method, the critical moment value for pure bending was $M_{max,kr}$ = 2.3161 kNm (Figure 21) (the number of buckling half-waves along the beam length was 10, and the buckling half-wave length was 42.0 mm). This means that the critical load values presented in Table 3 were approximately 30% lower than those obtained using the FSM method. In compression, the lowest critical load value was obtained for the overall beam buckling. This result is comparable to the finite strip method (Figure 22), which was P_{kr} = 5.474 kN.

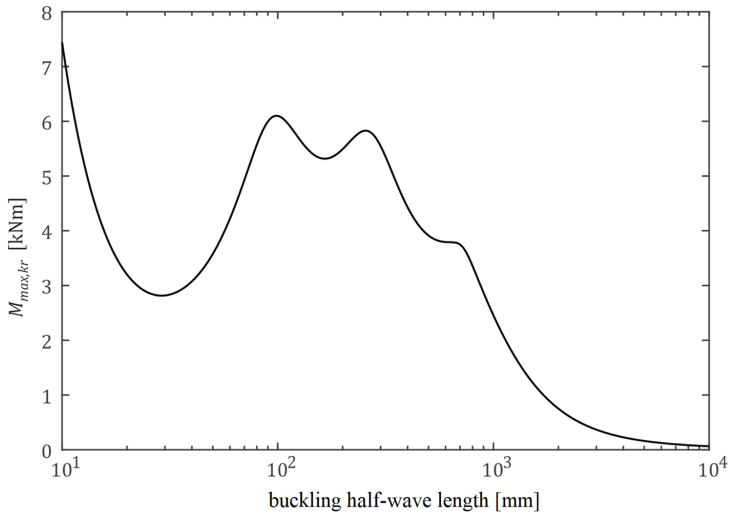

Figure 19. The critical moment diagram obtained by the finite strip method for the C2 profile in load case

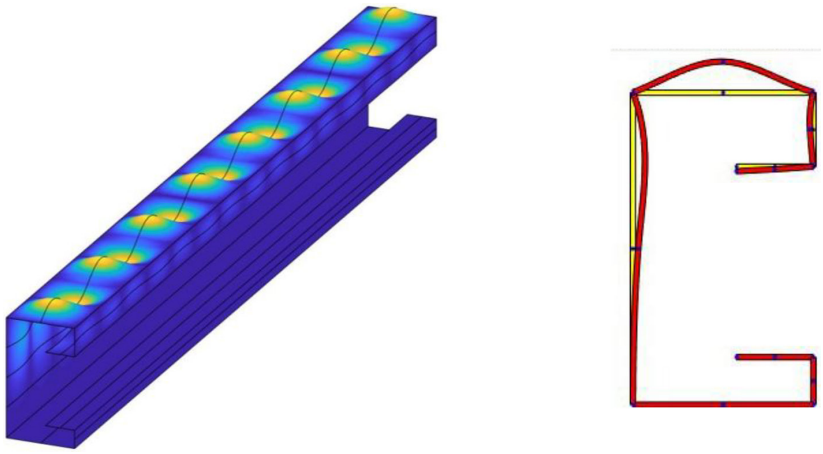

Figure 20. Buckling form obtained by the finite strip method (profile C2, load case I)

Table 3. Critical loads for profile Z1. In load cases I, II, III the beam length was L = 420 mm, in case IV L = 800 mm

Buckling form	Load case					
	I	II		III		IV
	$M_{max,kr}$ [kNm]	$M_{max,kr}$ [kNm]	q_{kr} [kN/m]	$M_{max,kr}$ [kNm]	F_{kr} [kN]	P_{kr} [kN]
Global	16.44	10.70	485.3	10.67	101.6	5.444
Distortional	0.2438	0.2166	9.823	1.075	10.24	8.719
Local	0.2502 (web)	0.2678 (web)	12.15 (web)	0.2957 (web)	2.816 (web)	20.93 (web)

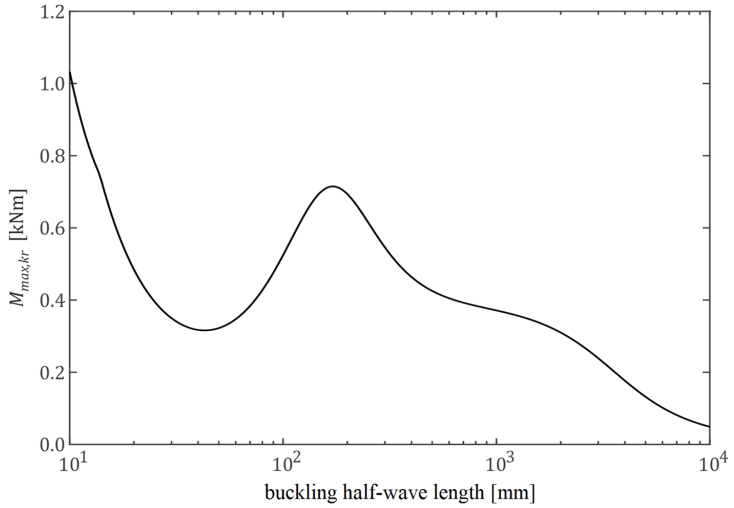

Figure 21. The critical moment diagram obtained by the finite strip method for profile Z1 in load case I

Table 4 presents the results obtained for the Z2-section. In bending, the lowest critical load value was obtained for the local stability mode (web buckling). Using the finite strip method, the critical moment value for pure bending was $M_{max,kr}$ = 0.9583 kNm (the number of buckling half-waves along the beam length was 8, and the buckling half-wave length was 52.5 mm). Therefore, the critical load values presented in Table 4 were approximately 23% lower than those obtained using the FSM method. In compression, the lowest critical load value was obtained for distortional buckling of the beam. This result is significantly lower than that obtained using the finite strip method, where the lowest critical force value was obtained for the global buckling mode of P_{kr} = 12.036 kN, which is practically the same as that obtained using the analytical method (Figures 23–28) .

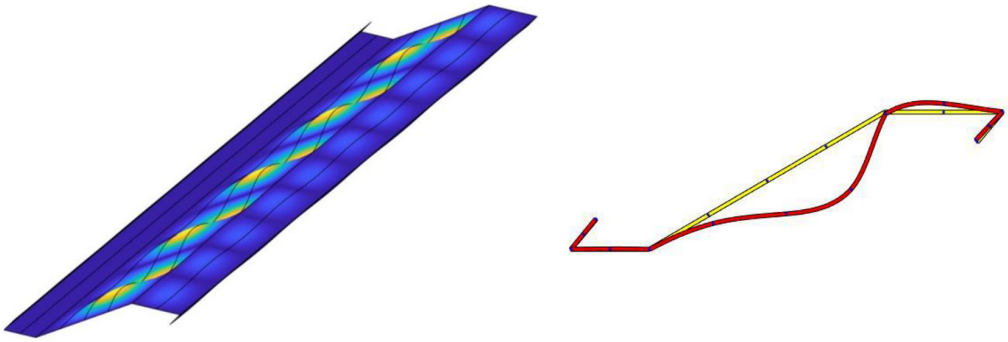

Figure 22. Buckling shape obtained using the finite strip method (profile Z1, load case I)

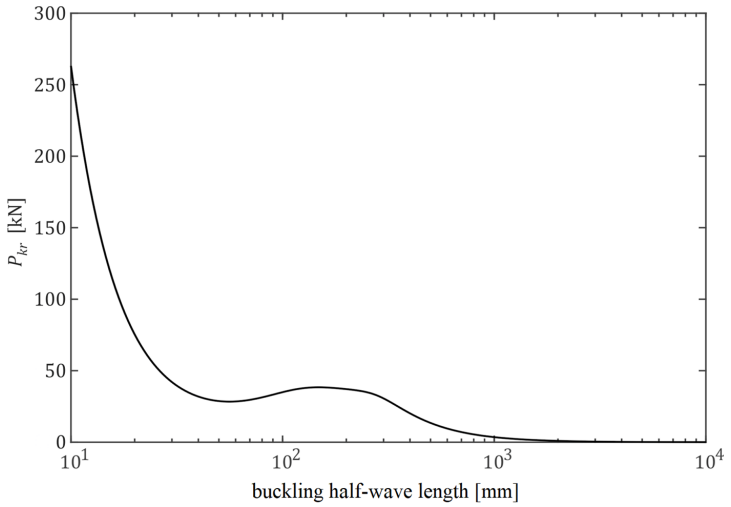

Figure 23. The critical force diagram obtained by the finite strip method for profile Z1 in the load case IV

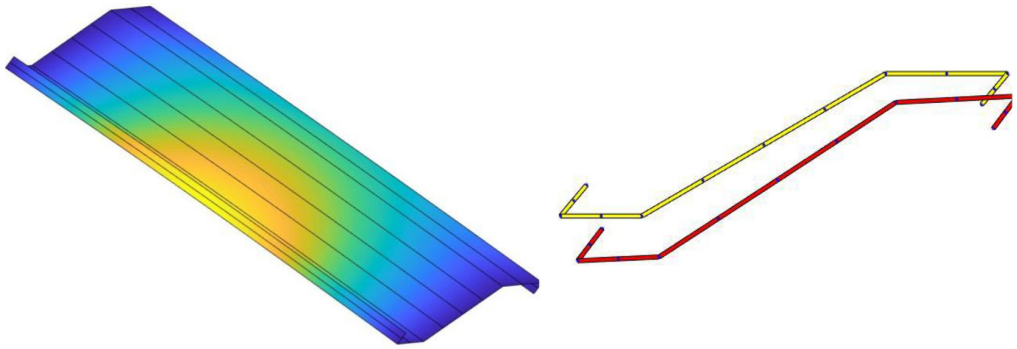

Figure 24. Buckling shape obtained using the finite strip method (profile Z1, load case IV)

A comparison of critical moments for different bending loads is shown in Figure 29. The analysis of these results shows clear differences in the resistance of the investigated cross-sections to local buckling under bending conditions. Among the examined variants, the highest values of the critical moment were obtained for cross-section C2. In all loading schemes considered, the values exceeded 2.0 kNm, reaching approximately 2.43 kNm in the case of a concentrated load applied at mid-span. This indicates that cross-section C2 exhibits the greatest resistance to local buckling and can be regarded as the most advantageous in terms of load-bearing capacity among the analyzed profiles.

The second highest performance was observed for cross-section Z2, for which M_{CR} ranged between approximately 0.7 and 0.9 kNm depending on the type of loading. Although these values are significantly lower than those

Table 4. Critical loads for profile Z2. In load cases I, II, III the beam length was L = 420 mm, in case IV L = 800 mm

Buckling form	Load case					
	I	II		III		IV
	$M_{max,kr}$ [kNm]	$M_{max,kr}$ [kNm]	q_{kr} [kN/m]	$M_{max,kr}$ [kNm]	F_{kr} [kN]	P_{kr} [kN]
Global	220.5	134.8	6113	128.6	1225	12.41
Distortional	-	-	-	-	-	1.708
Local	0.7354 (web)	0.8029 (web)	36.41 (web)	0.8979 (web)	8.551 (web)	29.340 (web)

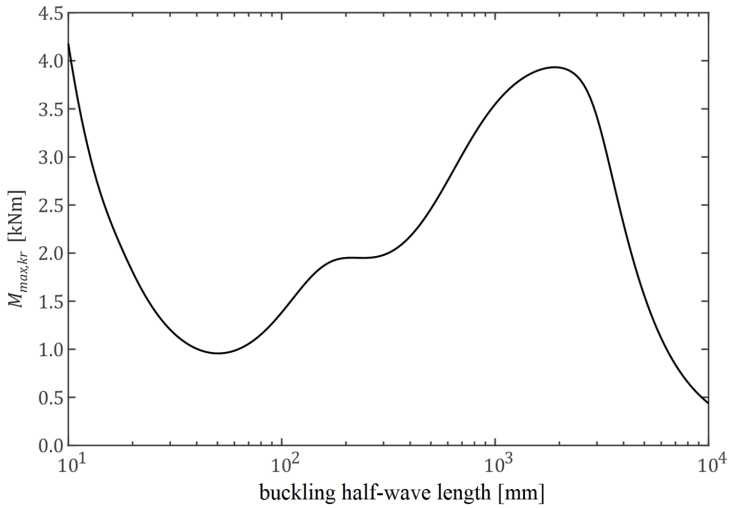

Figure 25. The critical moment diagram obtained by the finite strip method for the Z2 profile in load case I

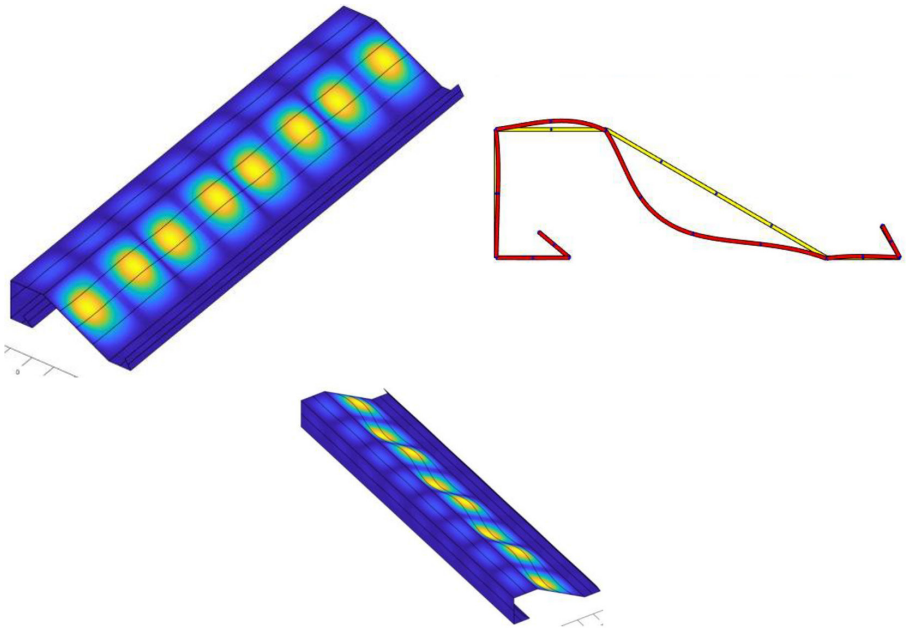

Figure 26. Buckling shape obtained using the finite strip method (profile Z2, load case I)

obtained for C2, cross-section Z2 demonstrates much better performance compared to cross-sections C1 and Z1. The latter are characterized by the lowest resistance to local buckling, with critical bending moment values not exceeding 0.55 kNm and with only minor differences between them. The influence of the loading scheme on M_{CR} is noticeable, particularly for cross-section C2, where the transition from moment loading to concentrated load results in an increase of

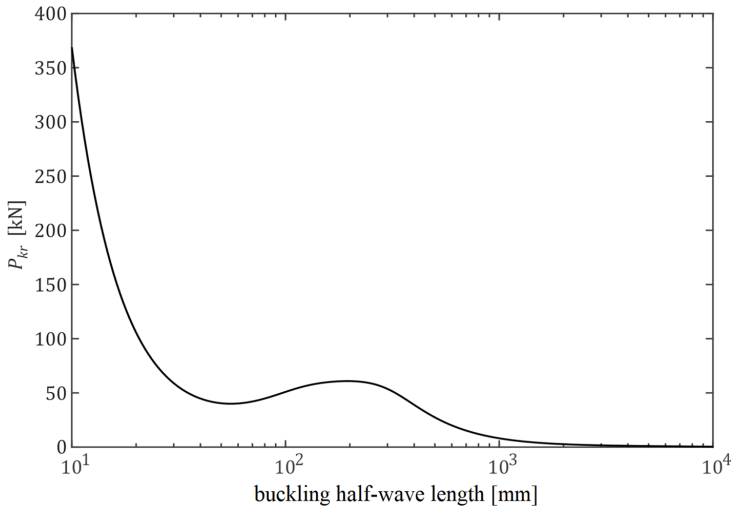

Figure 27. The critical force diagram obtained by the finite strip method for the Z2 profile in the IV load case

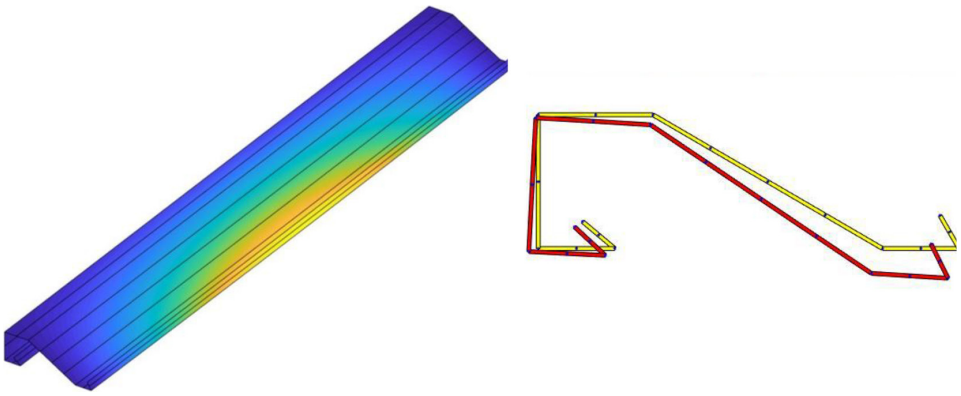

Figure 28. Buckling shape obtained using the finite strip method (profile Z2, load case IV)

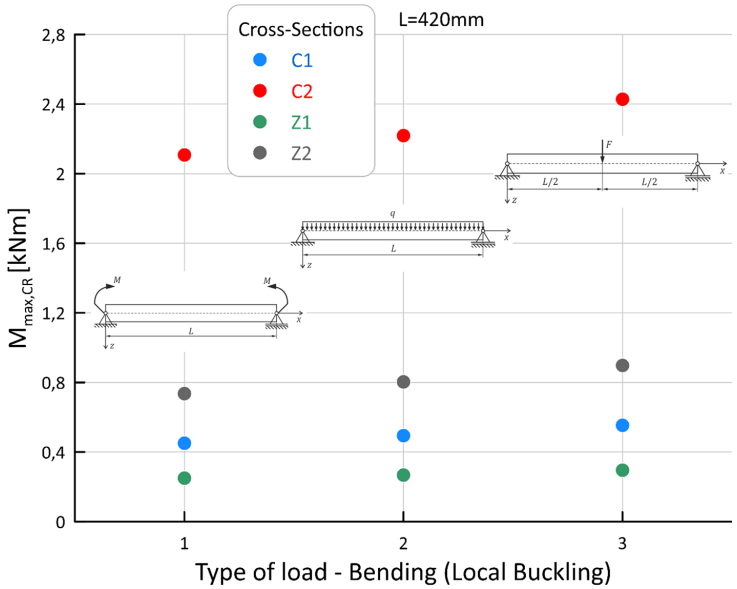

Figure 29. Comparison of critical moments for different loads

approximately 0.3 kNm in the critical value. In the case of cross-sections with lower resistance (C1 and Z1), this effect is minimal.

Figure 30 presents a comparison of critical forces for compression load. The highest values of the critical compressive force (F_{CR}) were

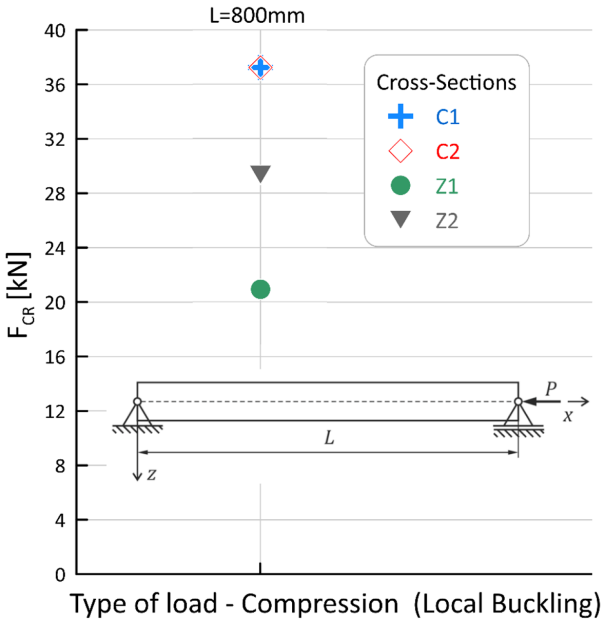

Figure 30. Comparison of critical forces for compression

obtained for cross-sections C1 and C2, both reaching 37 kN. The second highest performance was observed for cross-section Z2, which demonstrates a noticeably lower resistance to local buckling compared to C1 and C2, yet still relatively high. The critical compressive force reached approximately 29 kN, which is about 20% lower than that of the best-performing profiles. The lowest resistance was recorded for cross-section Z1, with F_{CR} of only about 21 kN. This value is nearly half of that obtained for C1 and C2, clearly limiting its suitability for applications involving significant compressive forces.

The analyses have shown that the resistance of the cross-sections to local buckling depends on the type of loading. Under bending, the best performance is demonstrated by cross-section C2, which achieves more than four times higher capacity compared to the weakest profiles (C1 and Z1). Under axial compression, the highest resistance to local buckling was obtained for cross-sections C1 and C2. Cross-section Z2 represents an intermediate solution in both cases, while Z1 proves to be the least favorable profile under both bending and compression.

CONCLUSIONS

The article focuses on the analysis of stability and load-bearing capacity of thin-walled beams with non-standard cross-sectional geometries, manufactured by Zaprom Sp. z o.o. The aim of the study was to determine the critical buckling loads under different loading conditions and to identify the dominant forms of instability. Analyses were carried out for three innovative profiles (channel and Z-sections), designed to enhance load-bearing efficiency and structural safety.

The research methodology combined a theoretical approach, based on the principle of potential energy conservation, with numerical calculations using the finite strip method (FSM). Four loading scenarios were considered: pure bending, uniformly distributed transverse load, concentrated force at mid-span, and axial compression. For each case, equilibrium equations were formulated, and critical buckling moments and forces were determined using the Bubnov-Galerkin method.

Three main forms of instability were distinguished: global (flexural–torsional), local (wall buckling), and distortional (cross-sectional deformation with flange displacement). The results showed that, for the analyzed profiles, the lowest critical loads were most often associated with local buckling of the walls, confirmed by both theoretical models and FSM calculations. In the case of axial compression, distortional or global buckling frequently governed the structural response.

The comparative analysis of profiles C1, C2, Z1, and Z2 highlighted significant differences between simplified analytical models and FSM

results, with discrepancies reaching 20–30%. This was mainly due to the inability of analytical models to fully capture the interaction of cross-sectional components. The most favorable buckling resistance was observed in profile C2, which demonstrated improved stability of the flanges.

The differences in the results obtained between analytical solutions and FSM are due to significant simplifications in the analytical model, e.g.: no interaction between individual buckling modes, in the case of distortional buckling, a section of the beam (flange) was isolated and assumed to be pinned at the edge of its connection with the web (interaction/cooperation with the rest of the cross-section was ignored), For local buckling, individual profile walls were considered separately and treated as plates pinned on four edges or three edges, and the fourth edge was free (the interaction between the walls was ignored).

The obtained results provide a basis for further optimization of thin-walled cross-sectional shapes, taking into account both load-bearing efficiency and structural safety. The combination of analytical methods with FSM enables a more precise assessment of beam behavior and facilitates the design of more efficient engineering solutions.

Acknowledgements

The project was funded by the National Science Centre, Poland allocated on the basis of the decision No. DEC-2021/43/B/ST8/00845 of 2022-05-23 – Contract No. UMO-2021/43/B/ST8/00845.

The paper is developed based on the statutory activity of the Poznań University of Technology (Grant of the Ministry of Science and Higher Education in Poland no 0612/SBAD/3640).

REFERENCES

1. Hancock GJ. Cold-formed steel structures. J Constr Steel Res. 2003;59(4):473–87, https://doi.org/10.1016/s0143-974x(02)00103-7
2. Pawlak AM, Górny TA, Plust M, Paczos P, Kasprzak J. Imperfections in thin-walled steel profiles with modified cross-sectional shapes - Current state of knowledge and preliminary studies. Steel Compos Struct. 2024;52(3):327–41, https://doi.org/10.12989/scs.2024.52.3.327
3. Magnucka-Blandzi E. Effective shaping of cold-formed thin-walled channel beams with double-box flanges in pure bending. Thin-Walled Struct. 2011;49(1):121–8, https://doi.org/10.1016/j.tws.2010.08.013
4. Magnucka-Blandzi E, Paczos P, Wasilewicz P. Buckling study of thin-walled channel beams with double-box flanges in pure bending. Strain. 2012;48(4):317–25, https://doi.org/10.1111/j.1475-1305.2011.00825.x
5. Jasion P, Pawlak A, Paczos P. Buckling and post-buckling behaviour of selected cold-formed C-beams with atypical flanges. Eng Struct. 2021;244:13, https://doi.org/10.1016/j.engstruct.2021.112693
6. Rhodes J, Seah LK. Buckling of edge-stiffened thin-walled beam sections. Proc Inst Civil Eng-Struct Build. 1992;94(3):323–34, https://doi.org/10.1680/istbu.1992.20292
7. Laudiero F, Zaccaria D. Finite-element analysis of stability of thin-walled-beams of open section. Int J Mech Sci. 1988;30(8):543–57, https://doi.org/10.1016/0020-7403(88)90098-7
8. Adany S, Schafer BW. Buckling mode decomposition of single-branched open cross-section members via finite strip method: Derivation. Thin-Walled Struct. 2006;44(5):563–84, https://doi.org/10.1016/j.tws.2006.03.013
9. Pawlak AM, Paczos P. Analysis of strength and resistance to loss of stability of thin-walled channel columns with non-standard cross-sectional shape. Arch Civ Eng. 2024;70(3):101–16, https://doi.org/10.24425/ace.2024.150973
10. SudhirSastry YB, Krishna Y, Budarapu PR. Parametric studies on buckling of thin walled channel beams. Comput Mater Sci. 2015;96:416–24, https://doi.org/10.1016/j.commatsci.2014.07.058
11. Grenda M, Paczos P. Experimental and numerical study of local stability of non-standard thin-walled channel beams. J Theor Appl Mech. 2019;57(3):549–62, https://doi.org/10.15632/jtam-pl/109601
12. Bourihane O, Ed-Dinari A, Braikat B, Jamal M, Mohri F, Damil N. Stability analysis of thin-walled beams with open section subject to arbitrary loads. Thin-Walled Struct. 2016;105:156–71, https://doi.org/10.1016/j.tws.2016.04.008
13. 13. Chu XT, Ye ZM, Li LY, Kettle R. Local and distortional buckling of cold-formed zed-section beams under uniformly distributed transverse loads. Int J Mech Sci. 2006;48(4):378–88, https://doi.org/10.1016/j.ijmecsci.2005.11.005
14. Kim NI, Shin DK, Park YS. Coupled stability analysis of thin-walled composite beams with closed cross-section. Thin-Walled Struct. 2010;48(8):581–96, https://doi.org/10.1016/j.tws.2010.03.006
15. Hancock GJ, Pham CH. Buckling analysis of thin-walled sections under localised loading using the semi-analytical finite strip method. Thin-Walled Struct. 2015;86:35–46, https://doi.org/10.1016/j.tws.2014.09.017

16. Pham DK, Pham CH, Hancock GJ. Explicit approach for elastic local buckling analysis of thin-walled channels under combined bending and shear. Thin-Walled Struct. 2022;173, https://doi.org/10.1016/j.tws.2022.108925
17. Magnucki K, Paczos P, Kasprzak J. Elastic buckling of cold-formed thin-walled channel beams with drop flanges. Journal Of Structural Engineering. 2010;136(7):886–96, https://doi.org/10.1061/(ASCE)ST.1943-541X.0000184
18. Penava DS, Radic A, Ilijas T. Elastic stability analysis of thin-walled c- and z-section beams without lateral restraints. Transactions of Famena. 2014;38(2):41–52.
19. Samanta A, Kumar A. Distortional buckling in monosymmetric I-beams. Thin-Walled Struct. 2006;44(1):51–6, https://doi.org/10.1016/j.tws.2005.09.007
20. Silvestre N, Camotim D. Distortional buckling formulae for cold-formed steel C and Z-section members Part I - derivation. Thin-Walled Struct. 2004;42(11):1567–97, https://doi.org/10.1016/j.tws.2004.05.001
21. Siva K, Visuvasam JA. Web-crippling behaviour of cold-formed screw fastened rectangular hollow flange z-section beams under two-flange load cases. Civil Engineering Journal. 2025;11(8):3186–207, https://doi.org/10.28991/CEJ-2025-011-08-07
22. Hulka I, Ungureanu V, Both I, Petzek E, Radu B. Influence of resistance spot welding parameters on cold-formed steel properties and failure modes. Civil Engineering Journal. 2025;11(6):2170–88, https://doi.org/10.28991/CEJ-2025-011-06-01
23. Pavlovic IR, Pavlovic R, Janevski G. Mathematical modeling and stochastic stability analysis of viscoelastic nanobeams using higher-order nonlocal strain gradient theory. Archives of Mechanics. 2019; 71(2): 137–53, https://doi.org/10.24423/aom.3139
24. Yu NT, Kim B, Yuan WB, Li LY, Yu F. An analytical solution of distortional buckling resistance of cold-formed steel channel-section beams with web openings. Thin-Walled Struct. 2019;135:446–52, https://doi.org/10.1016/j.tws.2018.11.012
25. Magnucka-Blandzi E. Critical state of a thin-walled beam under combined load. Appl Math Model. 2009;33(7):3093–8, https://doi.org/10.1016/j.apm.2008.10.014
26. Korobeynikov SN, Alyokhin VV, Annin BD, Babichev AV. Using stability analysis of discrete elastic systems to study the buckling of nanostructures. Archives Of Mechanics. 2012;64(4):367–404,
27. Binh PV, Duc NV, Sergeevich PV, Minh DB. Improved generalized procedure for determining critical state of a thin-walled beam under combined symmetric loads. International Journal Of Structural Stability And Dynamics. 2019;19(8), https://doi.org/10.1142/S0219455419500986
28. Pawlak AM, Paczos P, Grenda M, Górny TA, Rodak M. Mathematical and numerical analysis of local buckling thin-walled beams with non-standard cross-sections. Computers & Structures. 2025; 313, https://doi.org/10.1016/j.compstruc.2025.107752
29. Mohri F, Brouki A, Roth JC. Theoretical and numerical stability analyses of unrestrained, monosymmetric thin-walled beams. J Constr Steel Res. 2003;59(1):63–90, https://doi.org/10.1016/S0143-974X(02)00007-X
30. Li LY. Lateral-torsional buckling of cold-formed zed-purlins partial-laterally restrained by metal sheeting. Thin-Walled Struct. 2004;42(7):995–1011, https://doi.org/10.1016/j.tws.2004.03.005
31. Hancock GJ. Design for distortional buckling of flexural members. Thin-Walled Struct. 1997;27(1):3–12, https://doi.org/10.1016/0263-8231(96)00020-1
32. Schafer BW, Peköz T. Laterally braced cold-formed steel flexural members with edge stiffened flanges. Journal of Structural Engineering-Asce. 1999;125(2):118–27, https://doi.org/10.1061/(ASCE)0733-9445(1999)125:2(118)
33. Teng JG, Yao J, Zhao Y. Distortional buckling of channel beam-columns. Thin-Walled Struct. 2003;41(7):595–617, https://doi.org/10.1016/S0263-8231(03)00007-7
34. Jasion P, Pawlak AM, Paczos P, Plust M, Rodak M. Bending behaviour of thin-walled perforated channel beams with modified cross sectional shape – Part 2: analytical calculations and FEM. Bulletin of the Polish Academy of Sciences Technical Sciences. 2025;73(4):e153435, https://doi.org/10.24425/bpasts.2025.153435